INTERNATIONAL JOURNAL FOR NUMERICAL METHODS IN FLUIDS, VOL. 15, 411–426 (1992)

INVARIANT DISCRETIZATION OF THE INCOMPRESSIBLE NAVIER–STOKES EQUATIONS IN BOUNDARY FITTED CO-ORDINATES

A. SEGAL, P. WESSELING, J. VAN KAN, C. W. OOSTERLEE AND K. KASSELS

Delft University of Technology, Faculty of Technical Mathematics and Informatics, P.O. Box 5031, 2600 CD Delft, The Netherlands

SUMMARY

The discretization of the incompressible Navier–Stokes equation on boundary-fitted curvilinear grids is considered. The discretization is based on a staggered grid arrangement and the Navier–Stokes equations in tensor formulation including Christoffel symbols. It is shown that discretization accuracy is much enhanced by choosing the velocity variables in a special way. The time-dependent equations are solved by a pressure-correction method in combination with a GMRES method. Special attention is paid to the discretization of several types of boundary conditions. It is shown that fairly non-smooth grids may be used using our approach.

KEY WORDS Navier–Stokes equations Incompressible Boundary-fitted co-ordinates Boundary conditions Invariant discretization

1. INTRODUCTION

The numerical solution of the incompressible Navier–Stokes equations in complex geometries has long been a difficult problem for finite difference and finite volume techniques. During the last years, however, considerable attention has been focused on the discretization and solution of these equations in boundary-fitted co-ordinates.[1–9] Finite volume and finite difference discretization methods for the incompressible Navier–Stokes equations fall into two main classes: those using staggered and those using collocated (non-staggered) grids. Some publications in which staggered grids are used with general co-ordinates are References 1–5, 8 and 10. A staggered grid scheme using triangular volumes rather than quadrilaterals is described in Reference 11. Collocated grids with general co-ordinates are used in References 6, 7, 9 and 12–20. Furthermore, different sets of velocity unknowns may be chosen. The most commonly used velocity unknowns are Cartesian unknowns, contravariant and covariant unknowns. Rodi *et al.*4 give an excellent review over the various possibilities.

It is our final aim to solve the incompressible Reynolds-averaged time-dependent Navier–Stokes equations with turbulence modelling in complex 3D geometries. In this paper we restrict ourselves to 2D laminar flow as a first step. However, the methods described here will be constructed such that the extension to turbulent 3D flow is straightforward.

We have chosen staggered grids because of the inherent stability of the pressure approximation.[4] Furthermore, the time-accurate pressure-correction method as introduced by Chorin[21] is

0271–2091/92/160411–16$13.00

Received 19 September 1991
Revised 31 January 1992

used. To avoid possible instabilities in the pressure discretization, contravariant velocity unknowns are used instead of Cartesian velocity unknowns. As a consequence, the formulation contains Christoffel symbols, which may give rise to inaccuracies on non-smooth grids.

In Section 2 we recall some basic facts about the tensor formulation of the Navier–Stokes equations. In Section 3 the discretization of the incompressible Navier–Stokes equations in general co-ordinates by finite volume discretization is treated. It is shown that one should use fluxes through cell faces as unknowns rather than the contravariant velocity components. Furthermore, the satisfaction of a geometrical identity in discrete sense is essential for the success of the discretization. Section 4 is devoted to the treatment of the boundary conditions. Although this treatment does not get much attention in the literature, a correct implementation is crucial for the final solution. The time-accurate pressure-correction method in combination with linear solvers is the subject of Section 5. We use fully implicit linear solvers of conjugate gradient type. Numerical experiments show that these methods are quite suitable for solving the discrete equations. Finally, in Section 6 we present some test examples. It is demonstrated that, even for a very irregular grid, satisfactory results may be expected, and that the presence of Christoffel symbols does not lead to undue inaccuracies.

2. TENSOR FORMULATION OF THE NAVIER–STOKES EQUATIONS

In order to be able to deal with flow problems in domains of irregular geometry it is necessary to use grids that follow the boundaries accurately. We have decided to use finite volume techniques in combination with boundary-fitted co-ordinates. This means that the boundaries of the solution domain coincide with the grid lines. The physical domain is mapped onto a computational domain consisting of a number of rectangular blocks. Here we restrict ourselves to the one-block case, and to two dimensions.

The mapping $T: x \rightarrow \xi$ from an arbitrary domain Ω in the $\mathbf{x}$-plane to a rectangle G in the ξ-plane is assumed to be regular, which means that the Jacobian of the transformation is definite. In G a uniform computational grid is chosen. We assume that the only information about the mapping is the relation $\mathbf{x}=\mathbf{x}(\xi)$ in the grid points. The co-ordinates $\mathbf{x}$ are Cartesian.

A right-handed system of base vectors is assumed. To formulate the Navier–Stokes equations in curvilinear co-ordinates, tensor notation is of great help. Therefore, we recall some basic facts of tensor analysis. For an introduction to tensor analysis we refer to References 22–24. We introduce the covariant base vectors $\mathbf{a}_{(\alpha)}$ as

$$\mathbf{a}_{(\alpha)}=\frac{\partial x}{\partial \xi^{\alpha}}, \tag{1}$$

so that $\mathbf{a}_{(\alpha)}$ is tangent to the co-ordinate lines $\xi^{\beta}=\text{constant}$, $\beta \neq \alpha$, and the contravariant base vectors $\mathbf{a}^{(\alpha)}$ as

$$\mathbf{a}^{(\alpha)}=\nabla \xi^{\alpha}=\left(\frac{\partial \xi^{\alpha}}{\partial x^{1}}, \frac{\partial \xi^{\alpha}}{\partial x^{2}}\right)^{\mathrm{T}}, \tag{2}$$

so that $\mathbf{a}^{(\alpha)}$ is normal to the co-ordinate lines $\xi^{\alpha}=\text{constant}$.

The covariant and contravariant metric tensors $g_{\alpha\beta}$ and $g^{\alpha\beta}$ are defined by

$$g_{\alpha\beta}=\mathbf{a}_{(\alpha)} \cdot \mathbf{a}_{(\beta)}, \qquad g^{\alpha\beta}=\mathbf{a}^{(\alpha)} \cdot \mathbf{a}^{(\beta)}. \tag{3}$$

Let $g=\det(g_{\alpha\beta})$, then $\sqrt{(g)}$ equals the Jacobian of the transformation, $J=\det(\partial x/\partial \xi)$.

A covariant derivative is a tensor which reduces to a partial derivative of a vector field in Cartesian co-ordinates. For an absolute scalar, the covariant derivative is the same as the partial

derivative, and is denoted by

$$\mu_{,\alpha}=\frac{\partial\mu}{\partial\xi^{\alpha}}. \tag{4}$$

The covariant derivative of a contravariant tensor of rank one U^{α} is given by

$$U^{\alpha}_{,\beta}=\frac{\partial U^{\alpha}}{\partial\xi^{\beta}}+\left\{\begin{matrix}\alpha\\ \gamma\beta\end{matrix}\right\}U^{\gamma}, \tag{5}$$

where $\left\{\begin{matrix}\alpha\\ \gamma\beta\end{matrix}\right\}$ is the so-called Christoffel symbol of the second kind, defined by

$$\left\{\begin{matrix}\alpha\\ \gamma\beta\end{matrix}\right\}=\mathbf{a}^{(\alpha)}\cdot\frac{\partial\mathbf{a}_{(\gamma)}}{\partial\xi^{\beta}}=\frac{\partial\xi^{\alpha}}{\partial x^{\delta}}\frac{\partial^2 x^{\delta}}{\partial\xi^{\gamma}\partial\xi^{\beta}}=\frac{1}{2}g^{\alpha\delta}\left(\frac{\partial g_{\delta\gamma}}{\partial\xi^{\beta}}+\frac{\partial g_{\delta\beta}}{\partial\xi^{\gamma}}-\frac{\partial g_{\gamma\beta}}{\partial\xi^{\delta}}\right) \tag{6}$$

Furthermore, it can be shown that for a covariant derivative of a contravariant tensor of rank two $T^{\alpha\beta}$ the following relation holds:

$$T^{\alpha\beta}_{,\beta}=\frac{1}{\sqrt{(g)}}\frac{\partial\sqrt{(g)}T^{\alpha\beta}}{\partial\xi^{\beta}}+\left\{\begin{matrix}\alpha\\ \gamma\beta\end{matrix}\right\}T^{\gamma\beta}. \tag{7}$$

The incompressible Navier–Stokes equations in general co-ordinates are given by

$$U^{\alpha}_{,\alpha}=0, \tag{8}$$

$$\frac{\partial}{\partial t}(\rho U^{\alpha})+(\rho U^{\alpha}U^{\beta})_{,\beta}+(g^{\alpha\beta}p)_{,\beta}-\tau^{\alpha\beta}_{,\beta}=\rho f^{\alpha}, \tag{9}$$

where $\tau^{\alpha\beta}$ represents the deviatoric stress tensor

$$\tau^{\alpha\beta}=\mu(g^{\alpha\gamma}U^{\beta}_{,\gamma}+g^{\gamma\beta}U^{\alpha}_{,\gamma}), \tag{10}$$

with μ the viscosity, p the pressure, U^{α} the contravariant velocity component and ρ the density of the fluid. The contravariant velocity components and the Cartesian components are related by

$$\mathbf{u}=U^{\alpha}\mathbf{a}_{(\alpha)}. \tag{11}$$

An important relation is the so-called geometric identity

$$\oint_{\Gamma}a_{\beta}^{(\alpha)}\,\mathrm{d}\Gamma_{\alpha}=0 \tag{12}$$

for any physical volume Ω with surface Γ. Equation (12) can be derived by applying the divergence theorem in general co-ordinates to an arbitrary constant velocity field.

3. INVARIANT FINITE VOLUME DISCRETIZATION

Although invariant formulations are very attractive from a mathematical point of view, discretizations based on such a formulation seem complicated and costly, especially on staggered grids. For that reason many authors avoid completely invariant discretizations, for example, by using Cartesian velocity components. Rosenfeld *et al.*[25] have successfully discretized the incompressible Navier–Stokes equations in general co-ordinates, using Gibbs' notation. In this formulation Christoffel symbols do not occur explicitly. In our paper we follow a different approach, using tensor notation with explicit occurrence of Christoffel symbols but, as a consequence, obtaining smaller molecules. We shall show that such a discretization gives very satisfactory results if some precautions are taken.

x-plane

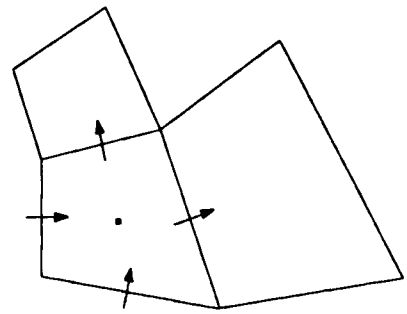

Figure 1. Staggered curvilinear grid (discretized)

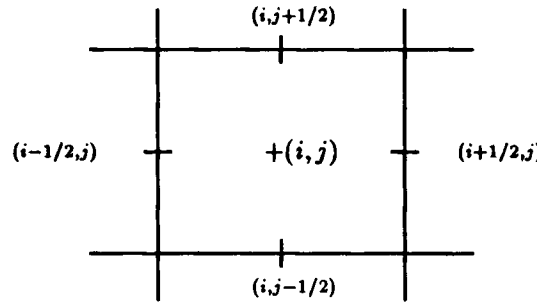

Figure 2. Numbering of points in a cell

In order to avoid possible pressure oscillations we use a staggered grid (Figure 1). The pressure is computed in the cell centres and the contravariant velocity components are used as unknowns at the centres of the cell faces. We number the nodes as indicated in Figure 2. The geometrical coefficients are computed by central differences and linear interpolation. From (1) it is clear that we can easily compute the following midside components of $\mathbf{a}_{(\alpha)}$:

$$a^{\alpha}_{(1)}(i, j \pm 1/2) \approx \frac{\delta x^{\alpha}}{\delta \xi^{1}}(i, j \pm 1/2), \qquad a^{\alpha}_{(2)}(i \pm 1/2, j) \approx \frac{\delta x^{\alpha}}{\delta \xi^{2}}(i \pm 1/2, j), \tag{13}$$

where $\delta x^{\alpha}(i, j \pm 1/2)$ and $\delta \xi^{1}(i, j \pm 1/2)$ are the increments of x^{α} and ξ^{1} in the positive ξ^{1}-direction along the face with centre $(i, j \pm 1/2)$, and similarly for $(i \pm 1/2, j)$.

From (13) one can approximate the value of $\mathbf{a}_{(\alpha)}$ in the centres of the cell and between neighbouring cells the lacking components at the centres of the cell faces by linear interpolation. The base vectors $\mathbf{a}^{(\alpha)}$ are computed from $\mathbf{a}^{(\alpha)} \cdot \mathbf{a}_{(\beta)} = \delta^{\alpha}_{\beta}$ and, so, metric tensors follow from (3). The Christoffel symbols contain second derivatives of the mapping (6) and, hence, are most sensitive to errors. Among the various possibilities we have found that a straightforward discretization of the first part of (6) gave the most satisfactory results. In the sequel we assume, without loss of generality, that the transformation is defined such that $\delta \xi^{1} = \delta \xi^{2} = 1$ for each cell.

In order to obtain accurate discretizations the following requirements should be met:

1. The geometric identity (12) should be exactly satisfied after discretization for all cells.
2. When representing a constant vector field **u** on the staggered grid in terms of its contravariant components U^α, and recomputing **u** from U^α, the original vector field **u** should be recovered exactly.

The first requirement is satisfied with our method of computation of the geometric quantities. The second requirement is less easily satisfied. Figure 3 shows a non-orthogonal grid in an L-shaped domain. Figure 4 shows a constant vector field and the same vetor field after transforming to the above staggered contravariant components in the cell-face centres and retransforming to Cartesian components in the cell vertices in an obvious way. Clearly, the non-uniformity in the grid produces large errors locally.

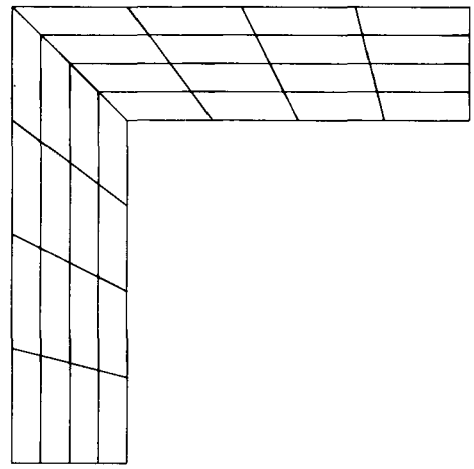

Figure 3. Grid for the L-shaped region

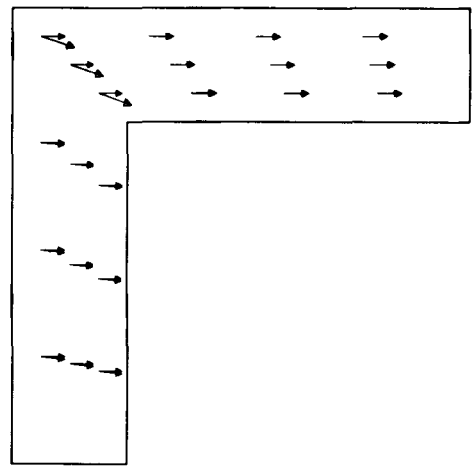

Figure 4. Constant velocity field before and after transformation operations

If we use $V^\alpha = \sqrt{(g)}U^\alpha$ as unknown, as proposed in Reference 25, and if we define $\sqrt{(g)}$ in the vertices of the cells by

$$\sqrt{(g)}_{i+1/2,\,j+1/2} = \frac{1}{4}\left\{\sum_2 a^1_{(1)} \sum_1 a^2_{(2)} - \sum_1 a^1_{(2)} \sum_2 a^2_{(1)}\right\}, \tag{14}$$

where $\sum_1$ denotes summation over the grid points $i+1/2, j$ and $i+1/2, j+1$ and $\sum_2$ summation over the grid points $i, j+1/2$ and $i+1, j+1/2$, then it is a straightforward exercise to show that the transformation $\mathbf{u} \to V^\alpha \to \mathbf{v}$ gives exactly $\mathbf{v} = \mathbf{u}$ if $\mathbf{u}$ is a constant vector. For this reason we shall use V^α as unknowns.

Next we consider the finite volume discretization of the continuity equation (7) and the momentum equations (9). Integration of the continuity equation over a cell with centre (i, j) and applying the Gauss divergence theorem gives

$$\int_\Omega U^\alpha_{,\alpha}\,\mathrm{d}\Omega = \int_\Gamma U^\alpha\,\mathrm{d}\Gamma_\alpha \approx V^1\big|^{(i,\,j+1/2)}_{(i,\,j-1/2)} + V^2\big|^{(i,\,j+1/2)}_{(i,\,j-1/2)}. \tag{15}$$

In compact notation (9) may be written as

$$T^{\alpha\beta}_{,\beta} = F^\alpha, \tag{16}$$

with

$$T^{\alpha\beta} = \rho U^\alpha U^\beta + g^{\alpha\beta} p - \tau^{\alpha\beta} \tag{17}$$

and

$$F^\alpha = \rho f^\alpha - \frac{\partial}{\partial t}(\rho U^\alpha). \tag{18}$$

Integration of (16) over a U^1-cell (see Figure 5) with centre $(i+1/2, j)$ and application of (7) gives $(\alpha = 1)$

$$\begin{aligned}\int_\Omega T^{\alpha\beta}_{,\beta}\,\mathrm{d}\Omega &= \int_\Omega \frac{\partial \sqrt{(g)}T^{\alpha\beta}}{\partial \xi^\beta}\,\mathrm{d}\xi^1\,\mathrm{d}\xi^2 + \int_\Omega \left\{\begin{matrix}\alpha\\ \gamma\beta\end{matrix}\right\} T^{\gamma\beta}\,\mathrm{d}\Omega \\ &\approx \sqrt{(g)}T^{\alpha_1}\big|^{(i+1,\,j)}_{(i,\,j)} + \sqrt{(g)}T^{\alpha_2}\big|^{(i+1/2,\,j+1/2)}_{(i+1/2,\,j-1/2)} + \left\{\begin{matrix}\alpha\\ \gamma\beta\end{matrix}\right\} T^{\gamma\beta}(i+1/2, j+1/2)\end{aligned} \tag{19}$$

and a similar expression for a U^2-cell may be derived.

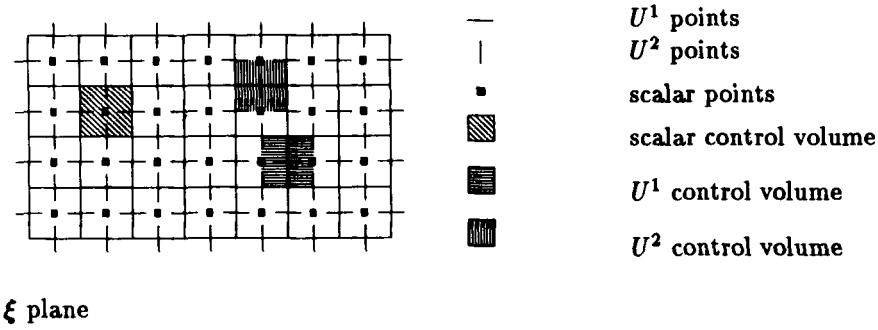

Figure 5. Arrangement of the unknowns for staggered grid

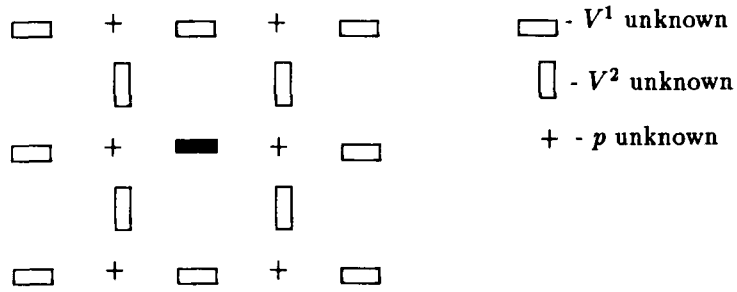

Figure 6. Stencil for momentum equations (V^1-cell)

The actual discretization may be derived by substituting (17) and (18) into (19) and substituting $V^\alpha = U^\alpha/\sqrt{(g)}$. The stencil corresponding to the V^1 molecule has been sketched in Figure 6; the V^2 stencil is obtained by rotation over 90°. In fact we have only a 19-point stencil (6 for pressure points, 13 for velocity points), which seems to be the absolute minimum for general co-ordinates in 2D.

4. TREATMENT OF THE BOUNDARY CONDITIONS

In the literature little information is given about boundary conditions in general co-ordinates. In this section we shall give an outline of how to treat several types of boundary conditions. We shall consider the following types of boundary conditions:

1. velocity prescribed
2. normal and tangential stresses prescribed
3. normal stress and tangential velocity given.

For ease of notation we shall restrict ourselves to a boundary part $\xi^2 = \text{constant}$; the case $\xi^1 = \text{constant}$ follows easily.

4.1 Prescribed velocities

In many practical problems the normal and tangential velocity components $\mathbf{u}\cdot\mathbf{n}$ and $\mathbf{u}\cdot\mathbf{t}$ are prescribed. To find the contravariant velocity components U^α, a transformation is necessary. Using tensor analysis one can show that for a boundary $\xi^2 = \text{constant}$, the following relations hold:

$$U^2 = \sqrt{(g^{22})}\,\mathbf{u}\cdot\mathbf{n}, \tag{20}$$

$$U^1 = \frac{1}{g_{11}}(\sqrt{(g_{11})}\,\mathbf{u}\cdot\mathbf{t} - g_{12}U^2). \tag{21}$$

Since the U^2-velocity component is situated at the boundary, no special treatment is necessary for this unknown. The U^1-component is present as virtual unknown, which may be eliminated by linear extrapolation from inner unknowns and the boundary value. Also the virtual pressure may be eliminated by linear extrapolation.

4.2. Normal and tangential stresses prescribed

Boundary conditions of the type normal and tangential stresses prescribed are sometimes used as outflow boundary conditions (see, for example, Reference 26), but may also be necessary for

multiblock methods on block boundaries. If we define S^{nn} and S^{nt} as the physical normal and tangential stress components then these boundary conditions are

$$S^{nn} \quad \text{and} \quad S^{nt} \text{ given.} \tag{22}$$

At the boundary $\xi^2 = \text{constant}$ σ^{21} and σ^{22} may be expressed in these quantities by the following transformation formulae:

$$\sigma^{22} = g^{22} S^{22}, \tag{23}$$

$$\sigma^{12} = (\sqrt{(g^{22} g_{11})} S^{21} - g_{21} \sigma^{22})/g_{11}, \tag{24}$$

where $\sigma^{\alpha\beta}$ is defined by

$$\sigma^{\alpha\beta} = -g^{\alpha\beta} p + \tau^{\alpha\beta}. \tag{25}$$

Since no velocity components are prescribed we need a control volume for all the unknowns, including the normal components lying at the boundary. The differential equation is only valid inside the domain; so, at the boundary we use half cell for the U^2-momentum equation. Figure 7 shows the grid at a lower boundary. From this figure it is clear that only the cells adjoining the boundary have a stencil extending outside the domain. For the shaded 'tangential' velocity cell in Figure 7 we distinguish between the contributions of the convection terms and those of the stress tensor. The convection term introduces virtual V^1-unknowns, as is clear from the figure. These unknowns may be eliminated by linear extrapolation.

With respect to the stress tensor we use formula (19) with $T^{1\beta}$ replaced by $\sigma^{1\beta}$; hence,

$$\int_\Omega \sigma^{1\beta}_{,\beta} \, d\Omega \approx \sqrt{(g)} \sigma^{11} \Big|_{(i,j)}^{(i+1,j)} + \sqrt{(g)} \sigma^{12} \Big|_{(i+1/2, j-1/2)}^{(i+1/2, j+1/2)} + \begin{Bmatrix} 1 \\ \gamma\beta \end{Bmatrix} \sigma^{\gamma\beta}_{(i+1/2, j+1/2)}. \tag{26}$$

The term $\sigma^{12}(i+1/2, j-1/2)$ may be replaced by the given boundary condition (24), the other terms are evaluated in the usual way with virtual velocities eliminated by linear extrapolation.

The 'half' cell for the U^2-momentum equation adjoining the boundary is sketched in Figure 8.

If we integrate (17) over the half cell we obtain

$$\int_\Omega T^{2\beta}_{,\beta} \, d\Omega = \int_\Omega \frac{\partial \sqrt{(g)} T^{2\beta}}{\partial \xi^\beta} d\xi^1 \, d\xi^2 + \int_\Omega \begin{Bmatrix} 2 \\ \gamma\beta \end{Bmatrix} T^{\gamma\beta} \, d\Omega. \tag{27}$$

A second-order accurate evaluation of (27) introduces extra points in the stencil and for that reason we make the following assumption: the natural boundary conditions S^{nt} and S^{nn} given, will

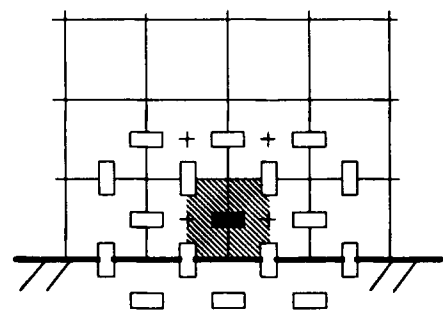

Figure 7. Grid at a 'lower' boundary in the computational domain. The last complete cell adjoining the boundary has been shaded

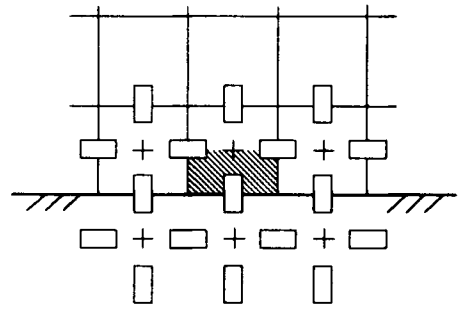

Figure 8. Half cell (shaded) adjoining 'lower' boundary in the computational grid

only be applied at the outflow boundaries, where the flow does not change much. This restriction allows us to evaluate integrals in (27) up to $O(h)$, instead of the usual $O(h^2)$ approximation. Hence, (27) may be approximated by

$$\int_\Omega T^{2\beta}_{,\beta}\,\mathrm{d}\Omega \approx \frac{1}{2}\sqrt{(g)}T^{21}\Big|^{(i+1/2,\,j-1/2)}_{(i-1/2,\,j-1/2)} + \sqrt{(g)}T^{22}\Big|^{(i,\,j)}_{(i,\,j-1/2)} + \frac{1}{2}\sqrt{(g)}\begin{Bmatrix}2\\ \gamma\beta\end{Bmatrix} T^{\gamma\beta}_{(i,\,j-1/2)}, \tag{28}$$

with $(i, j-1/2)$ the position of the V^2-unknown in the cell.

The contribution of the convection term is found by the substitution $T^{\alpha\beta}=\rho U^\alpha U^\beta$ and elimination of virtual velocities by linear extrapolation.

Setting $T^{\alpha\beta}=\sigma^{\alpha\beta}$ in (28) we get

$$\int_\Omega \sigma^{2\beta}_{,\beta}\,\mathrm{d}\Omega \approx \frac{1}{2}\sqrt{(g)}\sigma^{12}\Big|^{(i+1/2,\,j-1/2)}_{(i-1/2,\,j-1/2)} + \sqrt{(g)}\sigma^{22}\Big|^{(i,\,j)}_{(i,\,j-1/2)} + \frac{1}{2}\sqrt{(g)}\begin{Bmatrix}2\\ \gamma\beta\end{Bmatrix}\sigma^{\gamma\beta}_{(i,\,j-1/2)}. \tag{29}$$

The terms $\sigma^{12}(i-1/2, j-1/2)$, $\sigma^{22}(i-1/2, j-1/2)$, $\sigma^{12}(i, j-1/2)$ and $\sigma^{22}(i-1/2, j-1/2)$ are given by (23) and (24). The other terms contribute to the stencil in the usual way. The only extra problem is caused by the term

$$\frac{1}{2}\sqrt{(g)}\begin{Bmatrix}2\\ 11\end{Bmatrix}\sigma^{11}_{(i,\,j-1/2)}, \tag{30}$$

which requires the evaluation of $g^{12}\partial U^1/\partial\xi^2$ at the boundary. Since, for fixed i, only one U^1-unknown is present in the part of the stencil in the inner region, straightforward $O(h^2)$ approximation is not possible without enlarging the stencil. However, because we have already restricted ourselves to $O(h)$ approximation, approximate $U^1(i, j-1)$ by $U^1(i, j)$ which, in fact, means that we define

$$\frac{\partial U^1}{\partial \xi^2} \approx 0 \qquad \text{at the boundary.}$$

The error due to this assumption is small if U^1 does not change much in the direction of ξ^2 or if g^{12} is small, which implies that the outstream boundary is nearly straight. Other types of approximation are much more complicated and we expect that they do not give much more accuracy, under the circumstances assumed above.

4.3. Normal stress and tangential velocity prescribed

An alternative (commonly used) outflow condition is

$$\mathbf{u}\cdot\mathbf{t} \quad \text{and} \quad S^{nn} \text{ given.}$$

Unfortunately, in general $\mathbf{u}\cdot\mathbf{t}$ prescribed at a boundary $\xi^2=$ constant does not give U^1, because of the relation (21). Of course, if the grid is orthogonal at the outflow boundary, $g_{12}=0$ and (21) reduces to U^1 given. In a general grid we must either use (21) or we must use the boundary condition U^1 given. In general, the outflow boundary is artificial, and it is likely that the boundary condition U^1 given is as good or as bad as $\mathbf{u}\cdot\mathbf{t}$ prescribed. For that reason we restrict ourselves to the case U^1 prescribed instead of $\mathbf{u}\cdot\mathbf{t}$. With respect to the normal velocities we introduce half cells in the same way as before. The complete cell adjoining the boundary does not introduce any extra complications, except that virtual velocities and pressures must be eliminated by extrapolation. With respect to the half cell adjoining the boundary, we make again the $O(h)$ accuracy assumption which introduces (28). No further requirements are needed because the tangential velocity component is known at the boundary.

5. TIME DISCRETIZATION AND PRESSURE-CORRECTION METHOD

To solve the discrete equations (19) we use a standard time-accurate pressure-correction method as introduced by Chorin.[21] In our work we use the second-order accurate implementation described by Van Kan.[27] The spatial discretization described before results in a system of ordinary differential equations that may formally be written as

$$\begin{aligned}\mathbf{R}\dot{\mathbf{V}}_{\mathbf{M}}&=\mathbf{f}(\mathbf{V}_{\mathbf{M}},\mathbf{V}_{\mathbf{B}})+G\mathbf{P},\\ D_{\mathbf{M}}\mathbf{V}_{\mathbf{M}}+D_{\mathbf{B}}\mathbf{V}_{\mathbf{B}}&=0,\\ \mathbf{V}_{\mathbf{B}}&=\mathbf{g}(t),\end{aligned}\tag{31}$$

where $\mathbf{R}$ denotes the diagonal matrix containing ρ_i as the ith diagonal element, $\mathbf{V}_{\mathbf{M}}$ represents all non-prescribed fluxes ($V=\sqrt{(g)}U$), $\mathbf{P}$ represents the pressure unknowns, $\mathbf{f}$ represents the viscous stress as well as the convective terms and the volume forces, G represents the discretization of the gradient and $D=(D_{\mathbf{M}}, D_{\mathbf{B}})$ represents the divergence operator. The velocity unknowns $\mathbf{V}_{\mathbf{B}}$ are the ones that are prescribed at the boundary.

We use the so-called θ-method for the discretization of the time-derivatives. Application of the θ-method to (31) gives

$$\mathbf{R}\frac{\mathbf{V}_{\mathbf{M}}^{n+1}-\mathbf{V}_{\mathbf{M}}^{n}}{\Delta t}=\theta\mathbf{f}(\mathbf{V}_{\mathbf{M}}^{n+1},\mathbf{V}_{\mathbf{B}}^{n+1})+(1-\theta)\mathbf{f}(\mathbf{V}_{\mathbf{M}}^{n},\mathbf{V}_{\mathbf{B}}^{n})+\theta G\mathbf{P}^{n+1}+(1-\theta)G\mathbf{P}^{n},\tag{32}$$

$$\mathbf{V}_{\mathbf{B}}^{n+1}=g^{n+1},\tag{33}$$

$$D_{\mathbf{B}}\mathbf{V}_{\mathbf{B}}^{n+1}+D_{\mathbf{M}}\mathbf{V}_{\mathbf{M}}^{n+1}=0,\tag{34}$$

where n denotes the preceding time-level and $n+1$ the new time-level. In the pressure-correction method (32) and (33) are replaced by

$$\mathbf{R}\frac{\mathbf{V}_{\mathbf{M}}^{*}-\mathbf{V}_{\mathbf{M}}^{n}}{\Delta t}=\theta\mathbf{f}(\mathbf{V}_{\mathbf{M}}^{*},\mathbf{V}_{\mathbf{B}}^{*})+(1-\theta)\mathbf{f}(\mathbf{V}_{\mathbf{M}}^{n},\mathbf{V}_{\mathbf{B}}^{n})+G\mathbf{P}^{n},\tag{35}$$

$$\mathbf{V}_{\mathbf{B}}^{*}=g^{n+1}=\mathbf{V}_{\mathbf{B}}^{n+1}.\tag{36}$$

Subtracting (35) from (32) gives

$$\mathbf{R}\frac{\mathbf{V}_{\mathbf{M}}^{n+1}-\mathbf{V}_{\mathbf{M}}^{*}}{\Delta t}=\theta\mathbf{f}(\mathbf{V}_{\mathbf{M}}^{n+1},\mathbf{V}_{\mathbf{B}}^{n+1})-\theta\mathbf{f}(\mathbf{V}_{\mathbf{M}}^{*},\mathbf{V}_{\mathbf{B}}^{*})+\theta G(\mathbf{P}^{n+1}-\mathbf{P}^{n}).\tag{37}$$

Van Kan[27] shows that the term $\theta(\mathbf{f}(\mathbf{V}_{\mathbf{M}}^{n+1},\mathbf{V}_{\mathbf{B}}^{n+1})-\mathbf{f}(\mathbf{V}_{\mathbf{M}}^{*},\mathbf{V}_{\mathbf{B}}^{*}))$ may be neglected, without affect-

ing the order of accuracy. Hence, (37) is reduced to

$$\frac{\mathbf{V}_M^{n+1}-\mathbf{V}_M^*}{\Delta t}=\theta \mathbf{R}^{-1}G(\mathbf{P}^{n+1}-\mathbf{P}^n). \tag{38}$$

Applying the discrete divergence operator D_M to (38) gives

$$\frac{D_M\mathbf{V}_M^{n+1}-D_M\mathbf{V}_M^*}{\Delta t}=\theta D_M\mathbf{R}^{-1}G(\mathbf{P}^{n+1}-\mathbf{P}^n), \tag{39}$$

and because of (36) and (34), this may be written as

$$-\frac{D\mathbf{V}}{\Delta t}=\frac{-D_B\mathbf{V}_B^*-D_M\mathbf{V}_M^*}{\Delta t}=\theta D_M\mathbf{R}^{-1}G(\mathbf{P}^{n+1}-\mathbf{P}^n). \tag{40}$$

From equation (40) $\mathbf{P}^{n+1}-\mathbf{P}^n$ may be computed, and after that V_M^{n+1} results from (38). One easily verifies that the matrix $D_M\mathbf{R}^{-1}G$ corresponds to a nine-point molecule. Unfortunately the pressure matrix in (40) is non-symmetric for a non-orthogonal grid.

Equation (40) completely defines the pressure (up to a constant in the case of Dirichlet boundary conditions for the velocity), and no artificial pressure boundary condition is needed. The system of equations (40) is solved by a GMRES solver,[28] a projection type solver for non-symmetric matrices. To solve the non-linear system of equations (37) we use a Newton-linearization combined with the same GMRES solver.

6. SOME TEST RESULTS

To test the developed code we have run a number of test examples. The first problem is that of a 90° bend. Figure 9 shows the grid for the bend problem.

At the transition from curved to straight boundary the grid is non-orthogonal. Figure 10 shows the streamlines for this problem at $Re=500$ if we take U^α-unknowns. The outstream condition is tangential velocity zero and normal stress zero. At the instream a parabolic velocity profile is

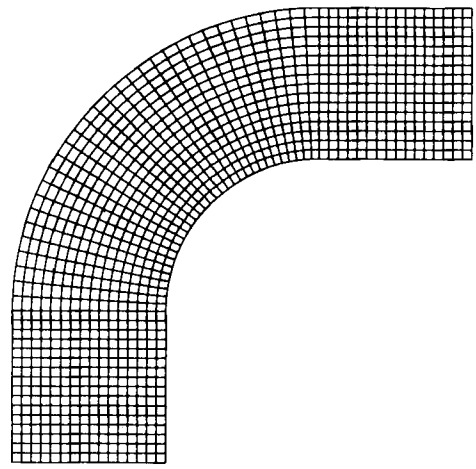

Figure 9. Mesh for 90° bend problem. Number of cells: 16 × 64

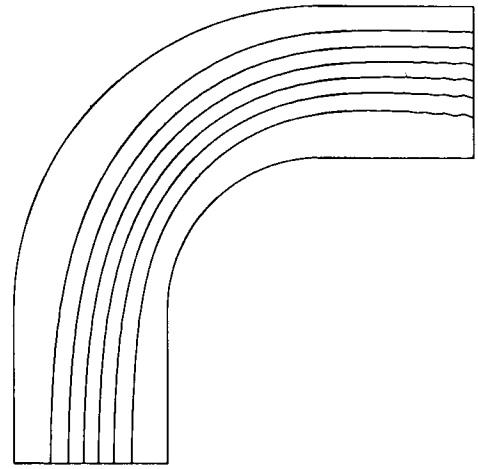

Figure 10. Streamlines for 90° bend problem at $Re = 500$. U^α-velocity unknowns

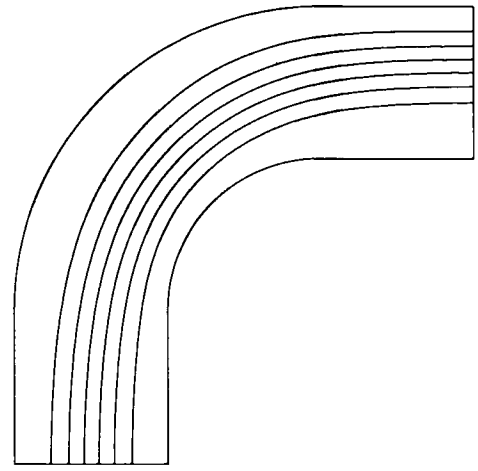

Figure 11. Streamlines for 90° bend problem at $Re = 500$. V^α-velocity unknowns

prescribed. Clearly in the neighbourhood of the outflow the streamlines show significant wiggles. The wiggles disappear if we use the V^α (flux)-unknowns (Figure 11).

More dramatic is the difference between the U^α- and V^α-unknowns for the L-shape domain of Figure 3. Figure 12 shows the velocity field with the U^α-unknowns for small Reynolds number ($Re = 10$). The same field with V^α-unknowns is given in Figure 13. The 'jump' in the grid at the bend (see Figure 3) introduces an unphysical recirculation region for the U^α-unknowns, which has disappeared completely with the V^α-unknowns. Finally, in Figures 14–16 we show the velocities, streamlines and isobars for a 180° bend at $Re = 500$, and in Figures 17 and 18 the streamlines and isobars for a skewed cavity at an angle of 63° and Reynolds number 1000. This last problem has been solved with a very fine grid (128×128).

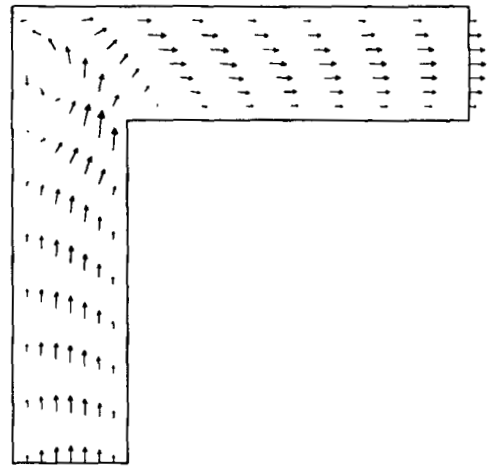

Figure 12. Velocity field in L-shaped region, $Re = 10$. U^e-unknowns

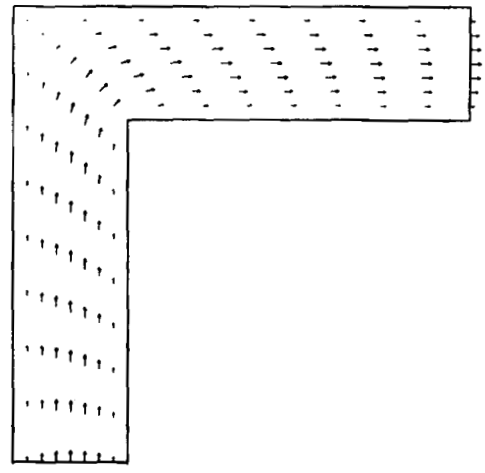

Figure 13. Velocity field for L-shaped region at $Re = 10$. V^e-unknowns

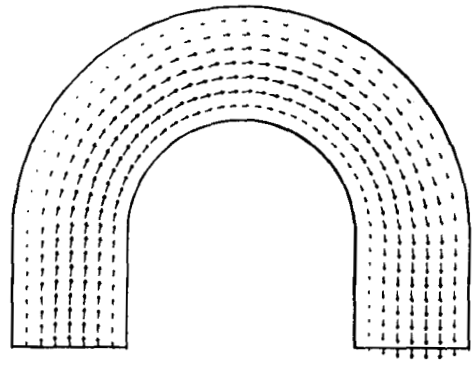

Figure 14. Velocity field in a 180° bend, $Re = 500$

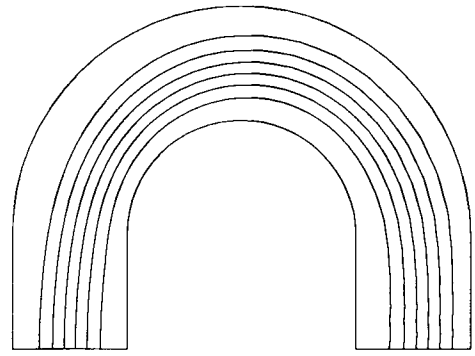

Figure 15. Streamlines in a 180° bend, $Re = 500$

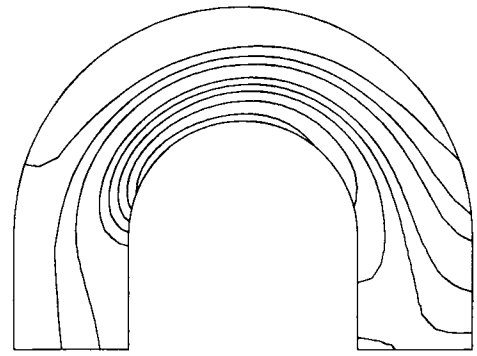

Figure 16. Isobars in a 180° bend, $Re = 500$

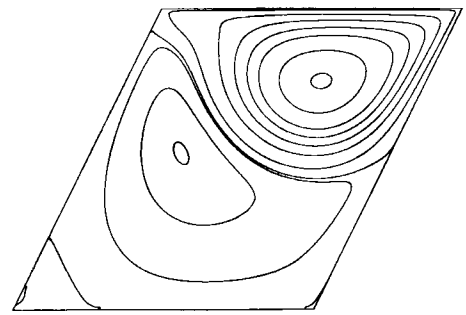

Figure 17. Streamlines for skewed cavity, $Re = 1000$, 128×128 grid

7. CONCLUSIONS AND FUTURE DEVELOPMENTS

The test examples shown in Section 6 indicate that our code is a reliable solver for the 2D incompressible Navier–Stokes equations on a curvilinear (non-orthogonal) grid. It has been demonstrated that the fluxes at cell boundaries ($\sqrt{(g)}U^\alpha$) should be used as unknowns instead of contravariant velocity unknowns U^α. The presence of Christoffel symbols in the formulae does

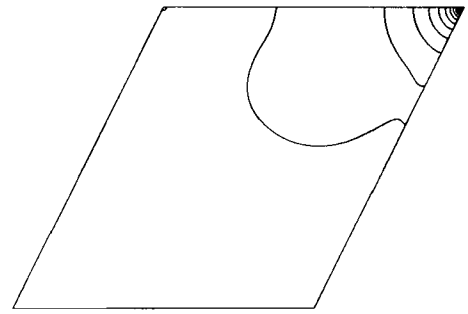

Figure 18. Isobars for skewed cavity, $Re = 1000$, 128×128 grid.

not allow us to use non-smooth co-ordinate mappings. Numerical experiments show that accurate results can be reached, provided the grid is fairly smooth. At this moment we are extending our code with a turbulence model (k–ε). Furthermore, we are investigating how the code may be improved in order that large differences in grid size (non-smooth co-ordinate mappings) can be handled accurately. Finally, the extension to 3D is under preparation.

REFERENCES

1. W. Shyy, S. S. Tong and S. M. Correa, 'Numerical recirculating flow calculation using a body fitted coordinate system', *Numer. Heat Transfer*, **8**, 99–113 (1985).
2. K. Katsuragi and O. Ukai, 'An incompressible inner flow analysis by absolute differential form of Navier–Stokes equation on a curvilinear coordinate system', in P. Wesseling (ed), *Proc. Eighth GAMM Conf. on Numer. Methods in Fluid Mechanics*, Notes on Numerical Fluid Mechanics 29, Vieweg, Braunschweig/Wiesbaden, 1990, pp. 233–242.
3. I. Demirdzic, A. D. Gosman, R. I. Issa and M. Perić, 'A calculation procedure for turbulent flow in complex geometries', *Comput. Fluids*, **15**, 251–273 (1987).
4. W. Rodi, S. Majumdar and B. Schönung, 'Finite volume methods for two-dimensional incompressible flows with complex boundaries', *Comput. Methods Appl. Mech. Eng.*, **75**, 369–392 (1989).
5. L. Davidson and P. Hedberg, 'Mathematical derivation of a finite volume formulation for laminar flow in complex geometries', *Int. j. numer. methods fluids*, **9**, 531–540 (1989).
6. M. Perić, R. Kessler and G. Scheuerer, 'Comparison of finite-volume numerical methods with staggered and collocated grids', *Comput. Fluids*, **16**, 389–403 (1988).
7. C. M. Rhie and W. L. Chow, 'Numerical study of the turbulent flow past an airfoil with trailing edge separation', *AIAA J.*, **21**, 1525–1532 (1983).
8. S. Koshizuka, Y. Oka and S. Kondo, 'A staggered differencing technique on boundary-fitted curvilinear grids for incompressible flows along curvilinear or slant walls', *Comput. Mech.*, **7**, 123–136 (1990).
9. E. Turkel, 'Preconditioned methods for solving the incompressible and low speed compressible equations', *J. Comput. Phys.*, **72**, 277–298 (1987).
10. H. Q. Yang, K. T. Yang and J. R. Lloyd, 'Buoyant flow calculations with non-orthogonal curvilinear co-ordinates for vertical and horizontal parallelepiped enclosures', *Int. j. numer. methods eng.*, **25**, 331–345 (1988).
11. R. A. Nicolaides, 'Flow discretization by complementary volume techniques', *AIAA Paper 89-1978*, Buffalo, New York, June 1989.
12. H. C. Chen and V. C. Patel, 'The flow around wing–body junctions', in *Fourth Symp. on Num. and Phys. Aspects of Aerod, Fl.*, Long Beach, U.S.A. 1989, pp. 1–15.
13. J. Piquet and P. Queutey, 'Computation of the viscous flow past a prolate spheroid at incidence', in P. Wesseling (ed), *Proc. Eighth GAMM Conf. on Numer. Methods in Fluid Mechanics*, Notes on Numerical Fluid Mechanics 29, Vieweg, Braunschweig/Wiesbaden, 1990, pp. 464–473.
14. J. Michelsen, 'Multigrid-based grid-adaptive solution of the Navier–Stokes equations', in P. Wesseling (ed), *Proc. Eighth GAMM Conf. on Numer. Methods in Fluid Mechanics*, Notes on Numerical Fluid Mechanics 29, Vieweg, Braunschweig/Wiesbaden, 1990, pp. 391–400.
15. W. Y. Soh and J. W. Goodrich, 'Unsteady solution of incompressible Navier–Stokes equations', *J. Comput. Phys.*, **79**, 113–134 (1988).
16. T. F. Miller and F. W. Schmidt, 'Use of a pressure-weighted interpolation method for the solution of the incompressible Navier–Stokes equations on a nonstaggered grid system', *Numer. Heat Transfer*, **14**, 213–233 (1988).

17. G. B. Deng, 'Numerical simulation of incompressible turbulent appendage–flat plate junction flows'. in C. Taylor, W. G. Habashi and M. M. Hafez (eds), *Numer. Methods in Laminar and Turbulent Flows, Vol. 6, Part 1*, Pineridge Press, 1989, pp. 793–803.
18. B. L. Lapworth, 'Examination of pressure oscillations arising in the computation of cascade flow using a boundary-fitted co-ordinate system', *Int. j. numer. methods fluids*, **8**, 387–404 (1988).
19. C. A. Hall, J. H. Ellison and T. A. Porsching, 'An unconditionally stable convergent finite difference method for Navier–Stokes problems on curved domains', *SIAM J. Numer. Anal.*, **24**, 1233–1248 (1987).
20. J. Piquet and M. Visonneau, 'Steady three-dimensional viscous fow past a shiplike hull', in M. Deville (ed), *Proc. Seventh GAMM Conf. on Numer. Methods in Fluid Mechanics*, Vieweg, Braunschweig, 1988, pp. 294–301.
21. A. J. Chorin, 'Numerical solution of the Navier–Stokes equations', *Math. Comput.*, **22**, 745–762 (1968).
22. R. Aris, *Vectors, Tensors and the Basic Equations of Fluid Mechanics*, Prentice-Hall, Englewood Cliffs, NJ, 1962.
23. L. I. Sedov, *A Course in Continuum Mechanics, Vol. I. Basic Equations and Analytical Techniques*, Wolters-Noordhoff Publishing, Groningen, The Netherlands, 1964.
24. I. S. Sokolnikoff, *Tensor Analysis*, Wiley, Englewood Cliffs, NJ, 1964.
25. M. Rosenfeld, D. Kwak and M. Vinokur, 'A solution method for the unsteady and incompressible Navier–Stokes equations in generalized coordinate systems', *AIAA Paper AIAA-88-0718*, 1988.
26. F. N. Van de Vosse, 'Numerical analysis of carotid artery flow', *Ph.D. Thesis*, Eindhoven University of Technology, The Netherlands, 1987.
27. J. J. I. M. Van Kan, 'A second-order accurate pressure correction method for viscous incompressible flow', *SIAM J. Sci. Stat. Comput.*, **7**, 870–891 (1986).
28. Y. Saad and M. H. Schultz, 'GMRES: a generalized minimal residual algorithm for solving non-symmetric linear systems', *SIAM J. Sci. Stat. Comput.*, **7**, 856–869 (1986).